Ecotoxicology and Environmental Safety 248 (2022) 114344

Contents lists available at ScienceDirect

Ecotoxicology and Environmental Safety

journal homepage: www.elsevier.com/locate/ecoenv

Multi-omics analysis reveals that iron deficiency impairs spermatogenesis by gut-hormone synthesis axis

Fa-Li Zhang [a,b], Shuai Yuan [a], Pei-Yu Dong [a], Hao-Hai Ma [a], Massimo De Felici [c], Wei Shen [b], Xi-Feng Zhang [a,*]

[a] College of Veterinary medicine, Qingdao Agricultural University, Qingdao 266100, China
[b] College of Life Sciences, Key Laboratory of Animal Reproduction and Biotechnology in Universities of Shandong, Qingdao Agricultural University, Qingdao 266109, China
[c] Department of Biomedicine and Prevention, University of Rome 'Tor Vergata', Rome 00133, Italy

ARTICLE INFO

Keywords:
Spermatogenesis
Iron deficiency
Multi-omics
CeRNA
Gut microbiome

ABSTRACT

Considering that research has mainly focussed on how excessive iron supplementation leads to reproductive cytotoxicity, there is a lack of in-depth research on reproductive system disorders caused by iron deficiency. To gain a better understanding of the effects of iron deficiency on the reproductive system, especially spermatogenesis, we first constructed a mouse model of iron deficiency. We employed multi-omic analysis, including transcriptomics, metabolomics, and microbiomics, to comprehensively dissect the impact of iron deficiency on spermatogenesis. Moreover, we verified our findings in detail using western blot, immunofluorescence, immunohistochemistry, qRT-PCR and other techniques. Microbiomic analysis revealed altered gut microbiota in iron-deficient mice, and functional predictive analysis showed that gut microbiota can regulate spermatogenesis. The transcriptomic data indicated that iron deficiency directly alters expression of meiosis-related genes. Transcriptome data also revealed that iron deficiency indirectly regulates spermatogenesis by affecting hormone synthesis, findings confirmed by metabolomic data, western blot and immunofluorescence. Interestingly, competing endogenous RNA networks also play a vital role in regulating spermatogenesis after iron deficiency. Taken together, the data elucidate that iron deficiency impairs spermatogenesis and increases the risk of male infertility by affecting hormone synthesis and promoting gut microbiota imbalance.

1. Introduction

Epidemiological studies have emphasised the growing problem of idiopathic infertility in men (Agarwal et al., 2021). It is generally considered that excessive or deficient iron intake is one of the factors that increase the risk of oxidative stress and thus the risk of abnormal sperm production (Wellejus et al., 2000; Madej et al., 2021). However, the mechanism by which inadequate iron intake affects spermatogenesis has not been elucidated.

Spermatogenesis, occurring in convoluted seminiferous tubules in testes, is a continuous process in which spermatogonia stem cells undergo proliferation, differentiation, meiosis and then form mature sperm (Nishimura and L'Hernault, 2017). Spermatogenesis is regulated by luteinising hormone (LH) and follicle-stimulating hormone (FSH) secreted by the pituitary gland, and testosterone secreted by Leydig cells (Khanehzad et al., 2021). The relationship between the gut microbiome and the reproductive system has also drawn increased attention (Ding et al., 2020; Zhang et al., 2022). Indeed, recent studies have confirmed that the gut microbiota is able to form a functionally complex and comprehensive three-dimensional network that regulates the reproductive, immune and metabolic systems. Moreover, the gut microbiota can act as protectors or invaders of the reproductive system (Boegehold et al., 2019; Zhang et al., 2021). Unfortunately, the characteristic changes in gut microbiota caused by iron deficiency have not been well described.

Iron deficiency anaemia, accounting for nearly half of the world's

Abbreviations: LH, Luteinising hormone; FSH, Follicle-stimulating hormone; FeD, iron-deficiency group; 16S-seq, 16S ribosomal DNA amplicon sequencing; DEGs, differentially expressed mRNAs; DELGs, differentially expressed lncRNAs; DEmiGs, differentially expressed miRNAs; GO, Gene Ontology; KEGG, Kyoto Encyclopedia of Genes and Genomes; RT-qPCR, Real-time quantitative polymerase chain reaction.

* Corresponding author.
E-mail addresses: zhangxf9465@163.com, zhangxf106@qau.edu.cn (X.-F. Zhang).

https://doi.org/10.1016/j.ecoenv.2022.114344
Received 17 September 2022; Received in revised form 22 November 2022; Accepted 24 November 2022
Available online 28 November 2022
0147-6513/© 2022 The Authors. Published by Elsevier Inc. This is an open access article under the CC BY-NC-ND license (http://creativecommons.org/licenses/by-nc-nd/4.0/).

anaemia cases, is the most common form of anaemia, with a prevalence of about 2% in adult men (Killip et al., 2007). Recent reports indicate that iron deficiency anaemia is one of the factors causing male infertility (Akhter et al., 2021). Micronutrients are necessary for good male reproductive health, and their deficiencies can lead to impaired male fertility. However, current attention is focussed on the dangers of excessive micronutrient intake (Guo et al., 2022; Peng et al., 2022). Here, in order to further understand the relationship between iron deficiency and gut microbiota imbalance, metabolic disorders and abnormal spermatogenesis, we adopted an integrated multi-omics approach. We found that iron deficiency can directly affect spermatogenesis and hormone synthesis–related gene expression. In addition, iron deficiency alters the microbiome, especially microbiota associated with spermatogenesis. We suggest that iron deficiency induces spermatogenesis dysfunction by promoting gut microbiota imbalance and affecting hormone synthesis.

2. Methods

2.1. Establishing an iron deficiency anaemia model in mice

All mice used in this study were ICR mice purchased from Qingdao Daren Fortune Animal Technology Co., Ltd.

Environmental conditions were 20–24 °C, humidity at 40–60%, a 12-hour photoperiod and free access to food and ultrapure water throughout the study period. Mice were isolated in stainless steel cages to prevent iron contamination. After three days of adaptive feeding, ICR mice were randomly divided into an iron-deficiency group (FeD) and a normal group (Control). The control group was fed a normal iron content, and the FeD group was fed low-iron feed (iron content of 12 ppm) for 8 weeks. Haemoglobin content is an important indicator of anaemia, and haemoglobin concentration < 9 g/dL indicates successful establishment of an iron deficiency anaemia model (Chen et al., 2021; Song et al., 2016). To determine whether our iron deficiency model was successful, we measured haemoglobin concentration in the blood of mice using a Veterinary Haematology Analyzer (Vetscan HM5, ABAXIS) after the fourth week of treatment (Supplementary Table S1).

2.2. Sample collection

Twelve hours before the mice were sacrificed, they were fasted but still allowed free access to water. The mice in each group were anaesthetised with ether in a fume hood. The retro-orbital venous plexus was used to collect blood, and after centrifugation to obtain serum, samples for LC-MS/MS were prepared. The contents of mouse small intestine were isolated and after quick freezing, samples for 16 S ribosomal DNA (rDNA) amplicon sequencing (16S-seq) were prepared. Testes were also collected for RNA extraction. After running quality control and constructing libraries, the samples were subjected to whole transcriptome sequencing, including mRNA, long noncoding RNA (lncRNA) and small RNA, among others.

2.3. mRNA sequencing analysis workflow

mRNA sequencing (mRNA-seq) was performed with an Illumina Hiseq 4000 platform and PE150 model by Beijing Novogene Technology Co., Ltd. (Beijing, China). The raw sequencing data went through a series of stringent quality controls before downstream analysis. Briefly, FastQC (v0.11.8) was used to check the data quality and inferior data were removed (Andrews, 2010). In addition, Fastp (v0.23.1) was used to filter low-quality, unqualified reads (Chen et al., 2018). Then, STAR (v 2.7.0 f) was selected to perform sequence alignment to a reference genome (Dobin et al., 2013). Finally, FeatureCounts (v1.6.3) was used to calculate the expression level of each gene or transcript (Liao et al., 2014).

2.4. lncRNA sequencing analysis workflow

Due to the specificity of library construction and other reasons, lncRNA sequencing (lncRNA-seq) and mRNA-seq data share an original file. Therefore, the quality control methods for lncRNA-seq data were similar to the quality control methods for mRNA-seq data. A difference was that after sequence alignment by using STAR (v 2.7.0 f), Stringtie (v1.3.4d) was used to splice transcripts (Dobin et al., 2013; Pertea et al., 2015). All transcripts were combined together and then compared using gffcompre (v0.10.6) and the reference annotation file. The candidate lncRNAs needs to meet the following conditions: i) the transcript annotated class code type was 'i, e, x, o, u'; ii) transcript length $\geq$ 200 bp, exons $\geq$ 2 and fragments per kilobase per million reads (FPKM) > 0.5; iii) the protein-coding ability of the transcript needs to be filtered by Coding Potential Calculator 2 (CPC2, v1.0.1), Coding-Non-Coding-Index (CNCI, python3 version) and pfamScan (v1.6) (Zhang et al., 2019; Kang et al., 2017; Sun et al., 2013). Similarly, FeatureCounts (v1.6.3) was used to calculate the expression level of each lncRNA (Liao et al., 2014).

2.5. Small RNA sequencing analysis workflow

The quality control methods of small RNA sequencing (miRNA-seq) were similar to the quality control methods of mRNA-seq data. Notably, miRNA-seq requires tighter quality control because the raw data are too short. The fastx-toolkit (v0.0.13) was used to trim bases. STAR (v 2.7.0 f) was selected to perform sequence alignment to mature mouse miRNA sequences from miRBase (http://www.mirbase.org/) (Dobin et al., 2013). Similarly, FeatureCounts (v1.6.3) was used to calculate the expression level of each miRNA (Liao et al., 2014).

2.6. Differential expression analysis of whole transcriptome sequencing

The DESeq2 (R package, v1.32.0) was used to evaluate differentially expressed genes, including mRNA (DEGs), lncRNAs (DELGs) and miRNAs (DEmiGs) (Love et al., 2014). To identify as many transcriptome changes caused by iron deficiency as possible, the standard for identifying DEGs was $|\log2\text{fold change [FC]}| > 0$ and $p < 0.05$.

2.7. Target gene prediction of noncoding RNAs

The *cis*- and *trans*-acting target genes of lncRNAs were predicted. *Cis*-acting means that the lncRNA regulates its neighbouring genes; we searched for genes within 10–100 kb (Zhang et al., 2019; Ling et al., 2017). *Trans*-acting refers to lncRNAs that regulate genes with the same or opposite expression patterns; we calculated the correlation between lncRNAs and mRNAs using Hmisc (v4.6–0, R package). The TargetScanMouse 8.0 database (https://www.targetscan.org/mmu_80/) was used to predict the target genes of miRNAs. Notably, miranda (v3.3a) was used to predict the relationship between miRNAs and lncRNAs.

2.8. Functional enrichment analysis of genes

The DEGs, DELGs and DEmiGs were used for functional enrichment analysis to identify significant regulatory signals. clusterProfiler (v4.0.5, R package) and Metascape (http://metascape.org/gp/index.html) were used to perform Gene Ontology (GO) and Kyoto Encyclopedia of Genes and Genomes (KEGG) pathway analysis (Wu et al., 2021; Zhou et al., 2019).

2.9. 16S-seq workflow

16S-seq was performed with Illumina NovaSeq platform and PE250 model by Beijing Novogene Technology Co., Ltd. Briefly, raw data were subjected to quality control and then FLASH (v1.2.11) was used to splice reads and to obtain raw tags. Fastp (v0.23.1) was used to filter low-quality tags (Chen et al., 2018). Usearch was used to compare the

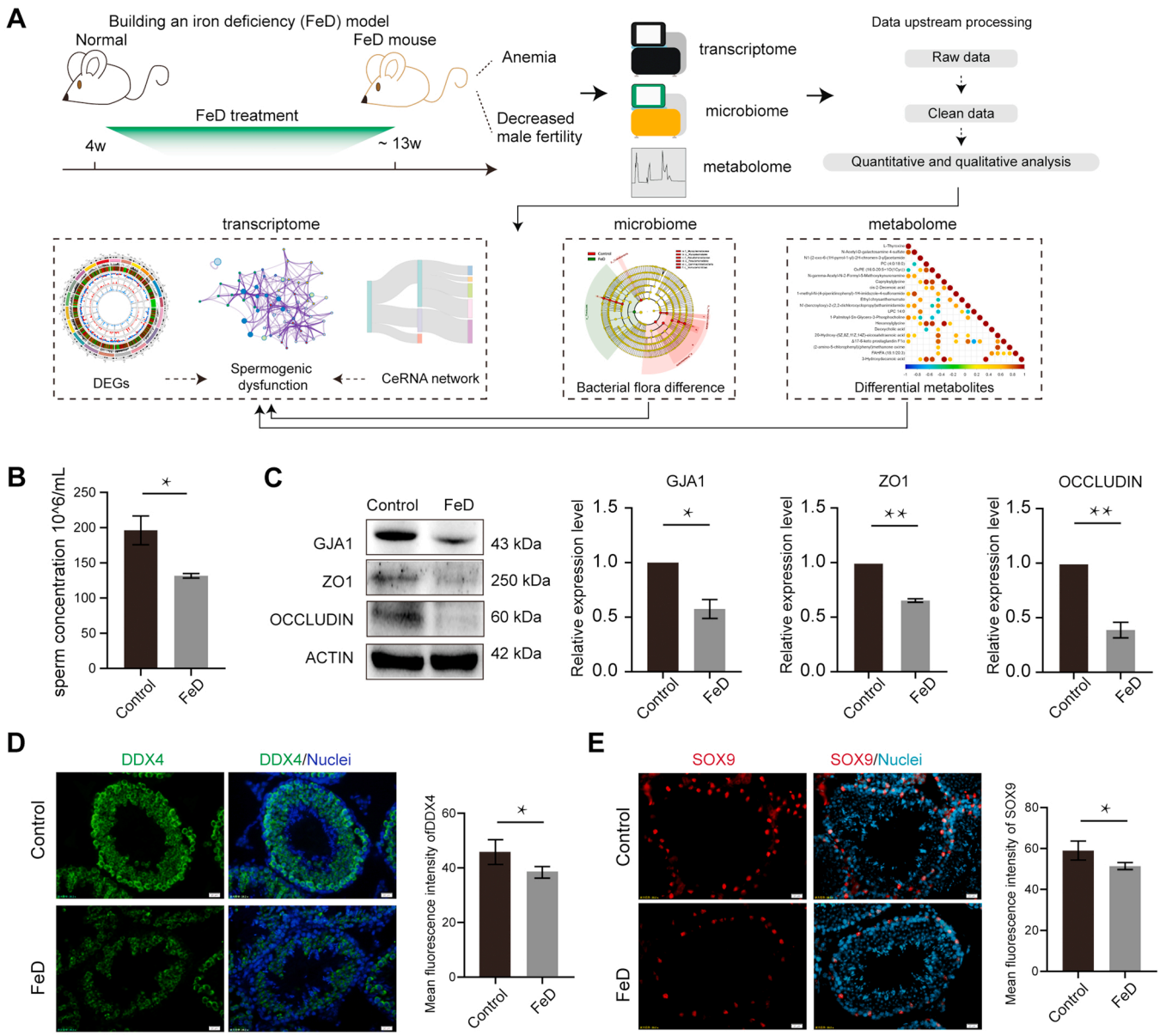

Fig. 1. Insufficient iron intake impairs spermatogenesis. (A) Establishing an iron deficiency (FeD) model and the experimental procedures of this study. Briefly, 4-week-old mice were given iron-deficient feed for 8 consecutive weeks, and the iron content in their blood was measured. The FeD model was successfully constructed once the iron concentration was < 9 g/dL. (B) The bar graph shows changes in the sperm concentration in iron-deficient mice. (C) Western blotting of GJA1, ZO1 and OCCLUDIN, spermatogenesis-related proteins. The bar graph shows the relative protein expression level. (D and E) Immunofluorescence of DDX4 and SOX9. The bar graph on the right shows the mean fluorescence density; The results were showed as mean ± SEM (n ≥ 3); * $p < 0.05$, * * $p < 0.01$ *vs.* the control group.

clean tags to the database to detect and remove chimeras. Moreover, the QIIME2 pipeline was adopted to carry out downstream analysis (Bolyen et al., 2019). Phylogenetic Investigation of Communities by Reconstruction of Unobserved Stats 2 (PICRUSt2, https://github.com/picrust/picrust2/wiki) was used for functional prediction (Douglas et al., 2020). Linear discriminant analysis effect size (LEfSe) and the T-test were used to identify differentially expressed microflora.

2.10. Metabolomic analysis workflow

Metabolomic analysis employed LC-MS/MS. The raw data were preprocessed using the Compound Discoverer 3.1 software. The spectra were compared with the high-quality mzCloud database constructed from standard materials and the mzVault and MassList databases to identify metabolites. Moreover, the metabolites were annotated based on KEGG analysis and the LIPID MAPS database. The differentially expressed metabolite screening thresholds were: variable importance in projection (VIP) > 1.0, FC > 1.2 or < 0.8 and $p < 0.05$. Notably, pos metabolites refer to some metabolites that are positively charged during mass spectrometry ionization, and neg metabolites refer to negatively charged metabolites.

2.11. Integrative analysis of 16S-seq and Metabolome

To measure the degree of association between species diversity and metabolites in environmental samples. Briefly, Pearson correlation analysis was performed between the significantly different flora obtained by 16S-seq and the significantly different metabolites obtained by metabolomics analysis.

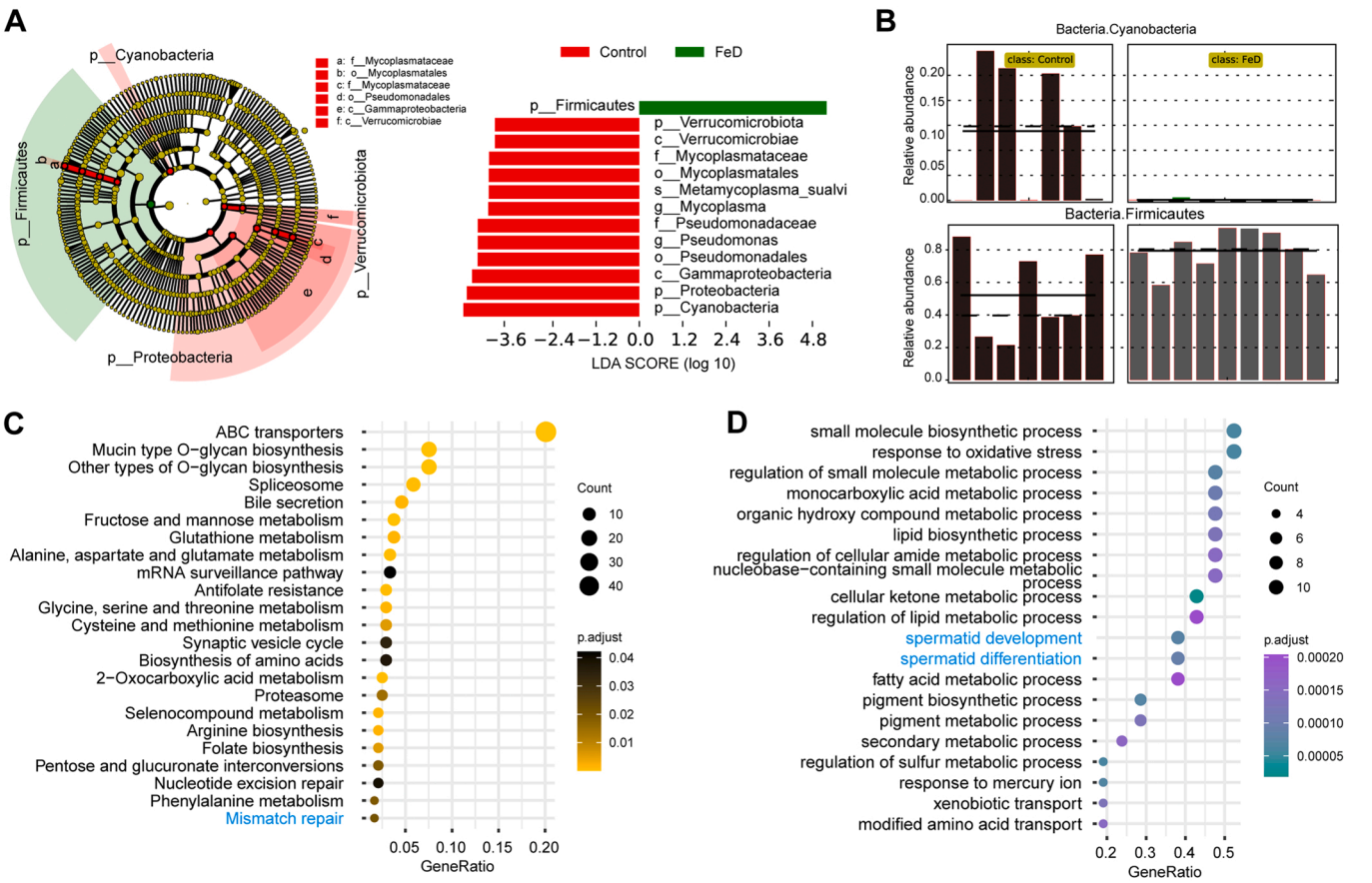

Fig. 2. Insufficient iron intake impairs gut microbiota homeostasis. (A) Cladogram of the FeD group *versus* the control group. Linear discriminant analysis effect size (LEfSe) was used to determine the differences in microbiota abundance; the same colour represents the same microbial taxon, and the dot size reflects the relative abundance at the same microbial taxonomic level. (B) The bar graph shows the relative abundance of the bacterial population; red means the control group and green means the FeD group. The upper panel is Cyanobacteria and the bottom panel is Firmicutes. (C) The dot plot shows the results of Gene Ontology (GO) analysis at the biological process level. (D) The dot plot shows the results of Kyoto Encyclopedia of Genes and Genomes (KEGG) analysis. The size of the point represents the number of genes, and the colour represents *p-adjust.*

2.12. Evaluation of sperm parameters

The tail of the epididymis was removed from the mouse and placed in a 3 cm Petri dish with 200 μL of preservation solution. The Petri dish was placed on a constant temperature heating table at 37 ℃, and the epididymis was cut with a scalpel. The sample was incubated for 5 min to completed release the sperm from the caudal epididymis. A pipette gun was used to transfer 20 μL of sperm storage solution and mix it with 200 μL of sperm storage solution. A pipette gun was used to transfer 4 μL of diluted sperm storage solution onto the sperm counting plate, and the sperm parameters were evaluated under a light microscope with the help of a computer-assisted sperm assay (CASA) system.

2.13. Detection of reproduction-related biochemical indexes by enzyme linked immunosorbent assay (ELISA)

Blood was collected from mice and used to isolate serum. The levels of reproductive factors in serum were determined using ELISAs kit (Solarbio, Shanghai, China). The contents of LH (JingMei, JM-11607M2, Jiangsu, China), testosterone (T) (JingMei, JM-02852M2, Jiangsu, China) and FSH (JingMei, JM-11681M2, Jiangsu, China) in serum were calculated based on absorbance at 450 nm measured by a spectrophotometer.

2.14. Immunohistochemistry

Immunohistochemical staining was performed as described previously (Kong et al., 2021). Briefly, after antigen retrieval and reaction with 3% H_2O_2, the samples were incubated with primary and second antibodies (see details in Supplementary Table S2). Finally, the samples were counterstained with haematoxylin. Using ImageJ software (version 1.53e), we determined the per cent of the area occupied by cells positive for the protein of interest.

2.15. Immunofluorescence

Immunofluorescence staining was performed as described previously (Zhang et al., 2019). Briefly, testicular tissue was fixed in paraformaldehyde overnight at 4 °C. Then, samples were dehydrated through a graded ethanol series, embedded in paraffin, rehydrated through a graded ethanol series and cut into 5-μm section. The sections were subjected to antigen retrieval and then incubated with the appropriate primary and secondary antibodies. Using ImageJ software (version 1.53e), we determined the per cent of the area occupied by cells positive for the protein of interest.

2.16. Real-time quantitative polymerase chain reaction (RT-qPCR)

All RNA was extracted and subsequently reverse transcribed into complementary DNA (cDNA) using the SPARKscript II one step RT-PCR kit (SparkJade, AG0401, Shandong, China). All primers are presented in Supplementary Table S3. RT-qPCR was performed with a Light Cycler 480 System (Roche, Germany) with SYBR Premix Ex Taq™ II (TAKARA, RR820A, Dalian, China). *Gapdh* and *U6* served as an internal reference to

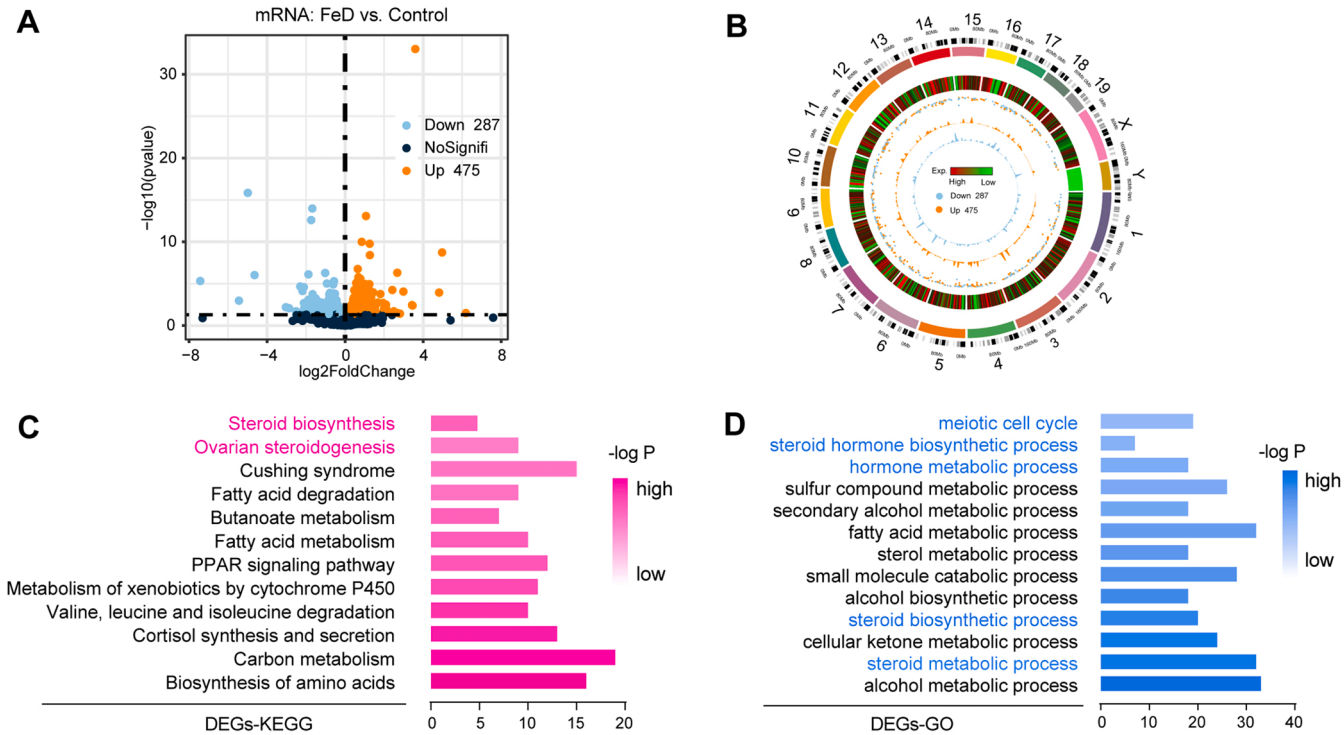

Fig. 3. Insufficient iron intake changes the transcriptomic landscape. (A) The volcano plot shows the differential expression levels of mRNAs in different groups. (B) The chord diagram shows the distribution and expression of each mRNA on the chromosomes. (C) The bar graph shows the results of Kyoto Encyclopedia of Genes and Genomes (KEGG) analysis of differentially expressed genes (DEGs). (D) The bar graph shows the results of Gene Ontology (GO) analysis of DEGs at the biological process level. The shade of the colour represents *p-adjust*.

calculate the relative expression level of genes using the $2^{-\Delta\Delta Ct}$ method.

2.17. Western blot

Western blotting was performed as described previously (Zhang et al., 2019). In brief, testis protein was extracted using radioimmunoprecipitation assay (RIPA) lysis buffer (Beyotime, Haimen, China, P0013C). The protein was separated with sodium dodecyl sulphate–polyacrylamide gel electrophoresis (Solarbio, S8010), however, due to the large span of the detected proteins, from 28 kDa to 250 kDa, we chose different separation gel concentrations when separating proteins. The 14% concentration was used to separate small proteins, while 8% and 10% were used to separate large proteins. Separated protein was transferred to membranes, which were blocked and then incubated with the appropriate primary and secondary antibodies (see details in Supplementary Table S2). The membranes were then exposed to a substrate to visual the protein bands. Using ImageJ software (version 1.53e), we determined the grey values of the protein bands to quantify expression.

2.18. Statistical analysis

The results are presented as the mean ± standard error of the mean (SEM) of at least three biological replications. The data were analysed with GraphPad Prism 8.0 (GraphPad Software, SanDiego, CA, USA). Student's t-test was used to compare between the groups. A p-value < 0.05 was considered significant.

3. Results

3.1. Iron deficiency impairs testicular development

To evaluate the effects of iron deficiency on testicular development, we established an iron-deficient mouse model and subjected it to multiomic analysis, including whole transcriptomics, microbiomics and metabolomics (Fig. 1A). We confirmed the iron- deficiency in the mouse model by examining the haemoglobin concentration in the blood (see details in 2.1 Establishing an iron deficiency anaemia model in mice). We then examined testicular development in the mice. The sperm concentration of FeD group mice was decreased significantly (Fig. 1B). We evaluated key testis structure-related proteins, including GJA1, ZO1 and OCCLUDIN, by western blot. Iron deficiency affected the development of the testis structure, resulting in a significant decrease in GJA1, ZO1 and OCCLUDIN (Fig. 1C). Based on immunofluorescence analysis, iron deficiency impaired germ cell development, denoted by decreased expression of DDX4 and SOX9, which are involved in testicular development (Fig. 1D and E).

3.2. Iron deficiency alters the gut microbiome

We performed 16S-seq to determine how iron deficiency influences the gut microbiome. The Firmicutes was the most abundant in all samples (Fig. S1A). The relative abundance of the top 35 microflora at the phylum level showed that Dependentiae was relatively high in several control samples and Halanaerobiaeota was relatively high in several FeD samples (Fig. S1B). When considering the average relative abundance, Halanaerobiaeota was higher in the FeD groups, and Firmicutes also had high expression (Fig. S1C). The amplicon sequence variant (ASV) analysis indicated there were 470 common ASVs between the FeD and control groups (Fig. S1D). As expected, Firmicutes expression was significantly higher in the FeD group (Fig. S1E). LEfSe analysis suggested that Firmicutes was highly expressed in the FeD group and Cyanobacteria was highly expressed in the control group (Fig. 2A). Specifically, the relative abundance of Firmicutes was about 60% higher in the FeD group than in the control group, while there was almost no Cyanobacteria in the FeD group (Fig. 2B). Notably, the function prediction analysis implied that changes in intestinal microflora induced by iron

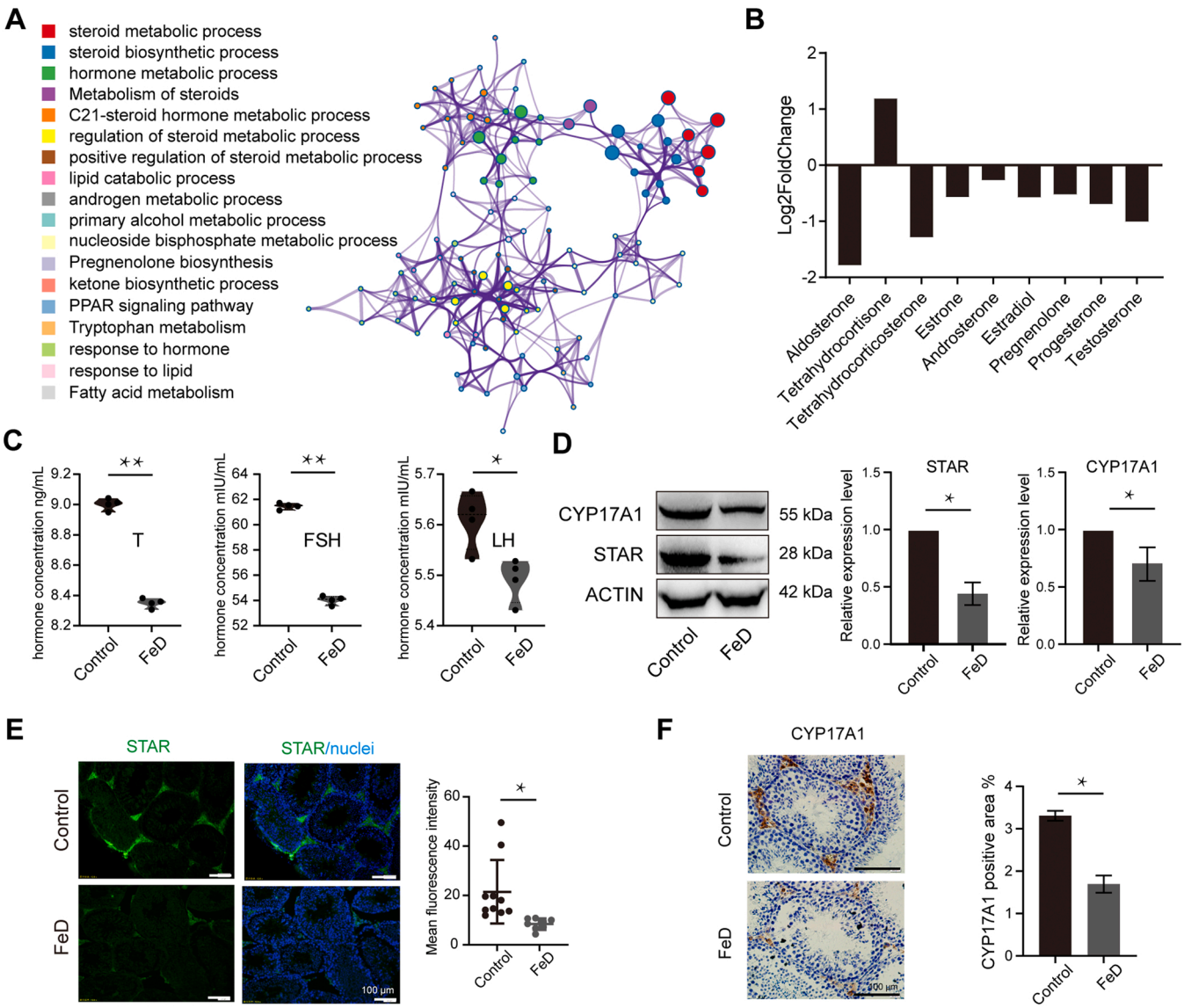

Fig. 4. Insufficient iron intake dysregulates hormone synthesis. (A) Kyoto Encyclopedia of Genes and Genomes (KEGG) and Gene Ontology (GO) analysis of differentially expressed genes (DEGs) after insufficient iron intake. (B) The bar graph shows the relative expression levels of hormones in the iron deficiency (FeD) group *versus* the control group detected by LC-MS/MS analysis. (C) The hormone levels in the blood; from left to right is testosterone (T), follicle-stimulating hormone (FSH) and luteinising hormone (LH), all determined with enzyme-linked immunosorbent assays. (D) Western blotting of hormone synthesis–related proteins. The bar graph shows the relative protein expression level. (E) Immunofluorescence of STAR (green) in the control and FeD groups. Hoechst 33342 (blue) was used to stain nuclei. The scale bar is 100 μm. The right panel represents the average fluorescence density of STAR in different groups. (F) Immunohistochemistry of CYP17A1 in the control and FeD groups. The scale bar is 100 μm. The right panel represents the CYP17A1-positive area in different groups. The results were showed as mean ± SEM (n ≥ 3); * $p < 0.05$, * * $p < 0.01$ *vs.* the control group.

deficiency could significantly affect spermatogenesis. Specifically, GO functional annotation indicated that microflora was related to mismatch repair (Fig. 2C), and KEGG metabolic pathway indicated that spermatid development was affected (Fig. 2D).

3.3. The influence of iron deficiency on gene transcription

To identify the influence of iron deficiency on gene transcription, we performed whole-transcriptome sequencing analysis, including mRNA-seq, lncRNA-seq and miRNA-seq. mRNA-seq revealed 762 DEGs, including 475 upregulated DEGs and 287 downregulated DEGs (Fig. 3A). Chromosomal mapping of DEGs suggested that genes on chromosome 3 were significantly different in expression (Fig. 3B). For lncRNA-seq, there were only 37 DELGs, with DELGs expressed on chromosome 17 having a tendency for higher expression (Fig. S2A and B). There were 17 DEmiGs; most showed a downward trend in the FeD group (Fig. S2E and F). To explore the functional changes in DEGs, DELGs and DEmiGs caused by iron deficiency, we conducted functional annotation analysis. The target genes of DEmiGs are associated with the FoxO signalling pathway (Fig. S2G). The target genes of DELGs are related to some metabolic processes and steroid biosynthesis (Fig. S2C andD). Interestingly, the KEGG pathway analysis of DEGs indicated that they participate in ovarian steroidogenesis and steroid biosynthesis (Fig. 3C). Finally, the GO analysis indicated that DEGs are involved in meiosis (Fig. 3D).

3.4. Effects of iron deficiency on hormone synthesis in mice

To assess the effects of iron deficiency on hormone synthesis in mice, we further explored the DEGs by using GO enrichment analysis. The

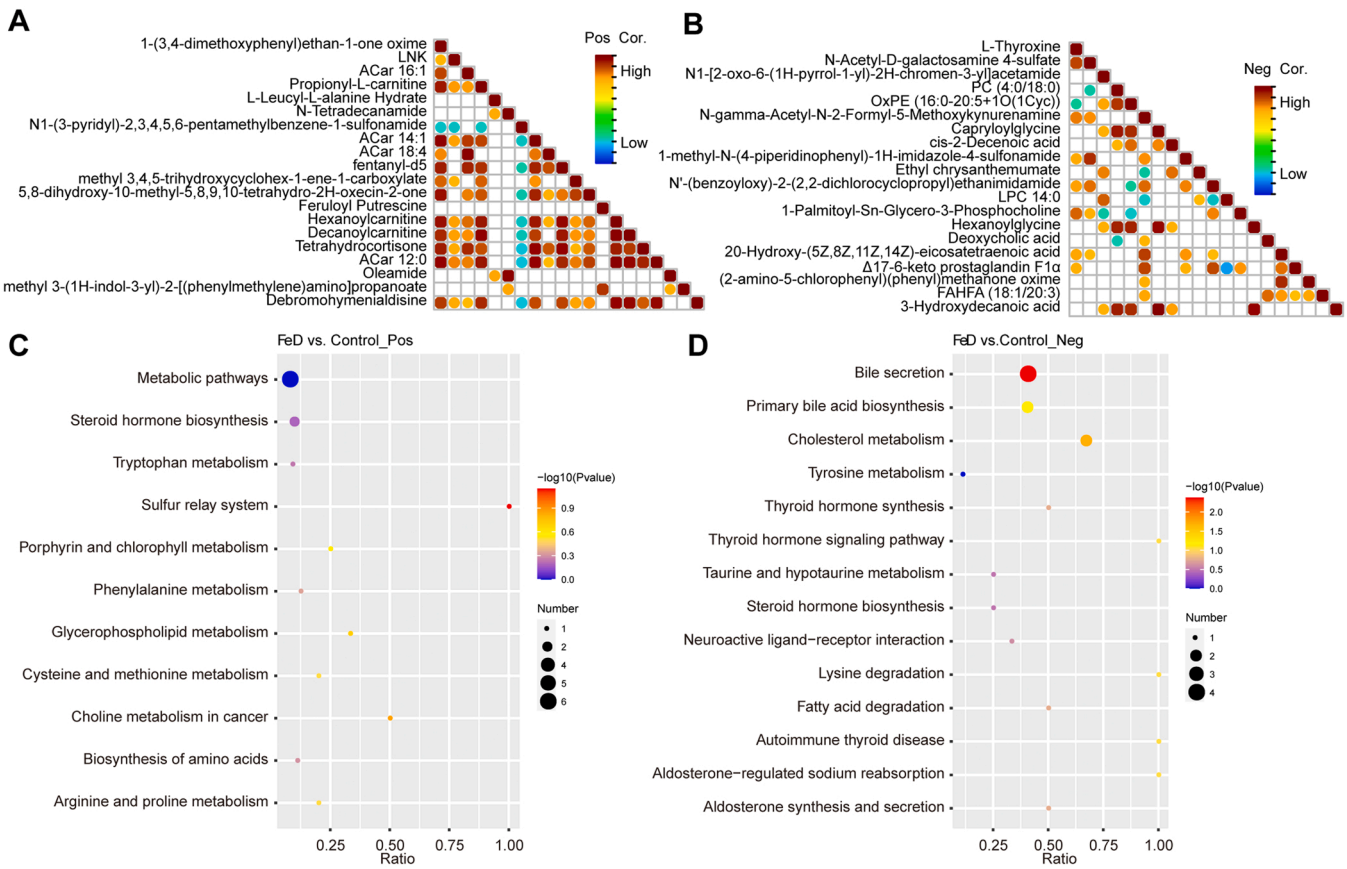

Fig. 5. Insufficient iron intake changes the metabolomic landscape. (A and B) Differential metabolite correlation analysis of the (A) positive ion mode and (B) negative ion mode. Red means positive correlation, blue means negative correlation. (C and D) Kyoto Encyclopedia of Genes and Genomes analysis of differential metabolite of the (C) positive ion mode and (D) negative ion mode. The colour represents *p*, and the size of the dots represents the number of metabolites.

results suggested that the DEGs participate in hormone metabolism (Fig. 4A). We analysed the metabolite levels by using LC-MS/MS. The metabolomic analysis suggested that there was decreased expression of hormones involved in regulating testicular development, such as T and estrone (Fig. 4B). Next, the T, FSH and LH levels in serum decreased significantly with iron deficiency (Fig. 4C).

Western blotting analysis verified the reduced steroidogenic acute regulatory protein (STAR) and cytochrome P450 17A1 (CYP17A1) expression (Fig. 4D). Immunofluorescence indicated that iron deficiency significantly reduced STAR (Fig. 4E). Immunohistochemistry showed that there was a trend for reduced CYP17A1 due to iron deficiency (Fig. 4F).

3.5. Effects of iron deficiency on metabolic processes in mice

We employed LC-MS/MS for metabolomic analysis. This approach provides substantial information regarding the metabolites in our samples and allowed us to assess how iron deficiency affected metabolism, including hormone metabolism. First, we compared our spectra to the LIPID MAPS database, which is the largest public LIPID database. For pos metabolites, there were six metabolite clusters, including fatty acyls, glycerolipids, glycerophospholipids, polyketides, prenol lipids, sphingolipids and sterol lipids (Fig. S3A). For pos metabolites, there were five metabolite clusters, including fatty acyls, glycerophospholipids, polyketides, prenol lipids and sterol lipids (Fig. S3B). Principal component analysis indicated that iron deficiency has a marker impact on metabolism, including pos and neg metabolites (Fig. S3C and D). We evaluated 79 neg and 39 pos metabolites (Fig. S3E and F). Correlation analysis revealed larger correlations for some metabolites, such as Oleamide/N-Tetradecanamide, 3-hydroxydecanoic acid/Capryloylglycine, suggesting that these metabolites play a synergistic role (Fig. 5A and B). Interestingly, the function prediction of differentially expressed metabolites indicated that both pos and neg metabolites participate in steroid hormone biosynthesis (Fig. 5C and D).

3.6. Integrative analysis of iron deficiency on gut microbes and blood metabolites

To explore whether changes in the gut environment affect metabolites, we performed correlation analysis between differentially expressed gut microbiota and differential metabolites in blood after iron deficiency. Here, there was a good correlation between blood metabolome and gut microbiota. *Agathobacter* and *Coprococcus* were positively correlated with most of the metabolites. However, *Nitrosarchaeum* was negatively correlated with most of the neg metabolites (Fig. 6A and B).

3.7. Iron deficiency impairs spermatogenesis

Transcriptomic analysis suggested that iron deficiency can directly impair the transcription of genes related to spermatogenesis. To determine the impact of iron deficiency on spermatogenesis, we first conducted functional enrichment analysis on DEGs. Bioinformatic analysis showed that iron deficiency directly altered DNA repair, meiosis and cell division, among others (Fig. 7A). Interestingly, the gene expression trend analysis showed that most DEGs involved in spermatogenesis, like *Dazl* and *Sycp1*, were downregulated in the presence of iron deficiency (Fig. S4A). Non-coding RNAs play a vital role in regulating spermatogenesis. We built a ceRNA network of non-coding and coding RNAs that regulate spermatogenesis and hormone formation. It revealed that the *miR-128–3p/Mybl1/MSTRG.15485* and *miR-542–3p/Sun2/*

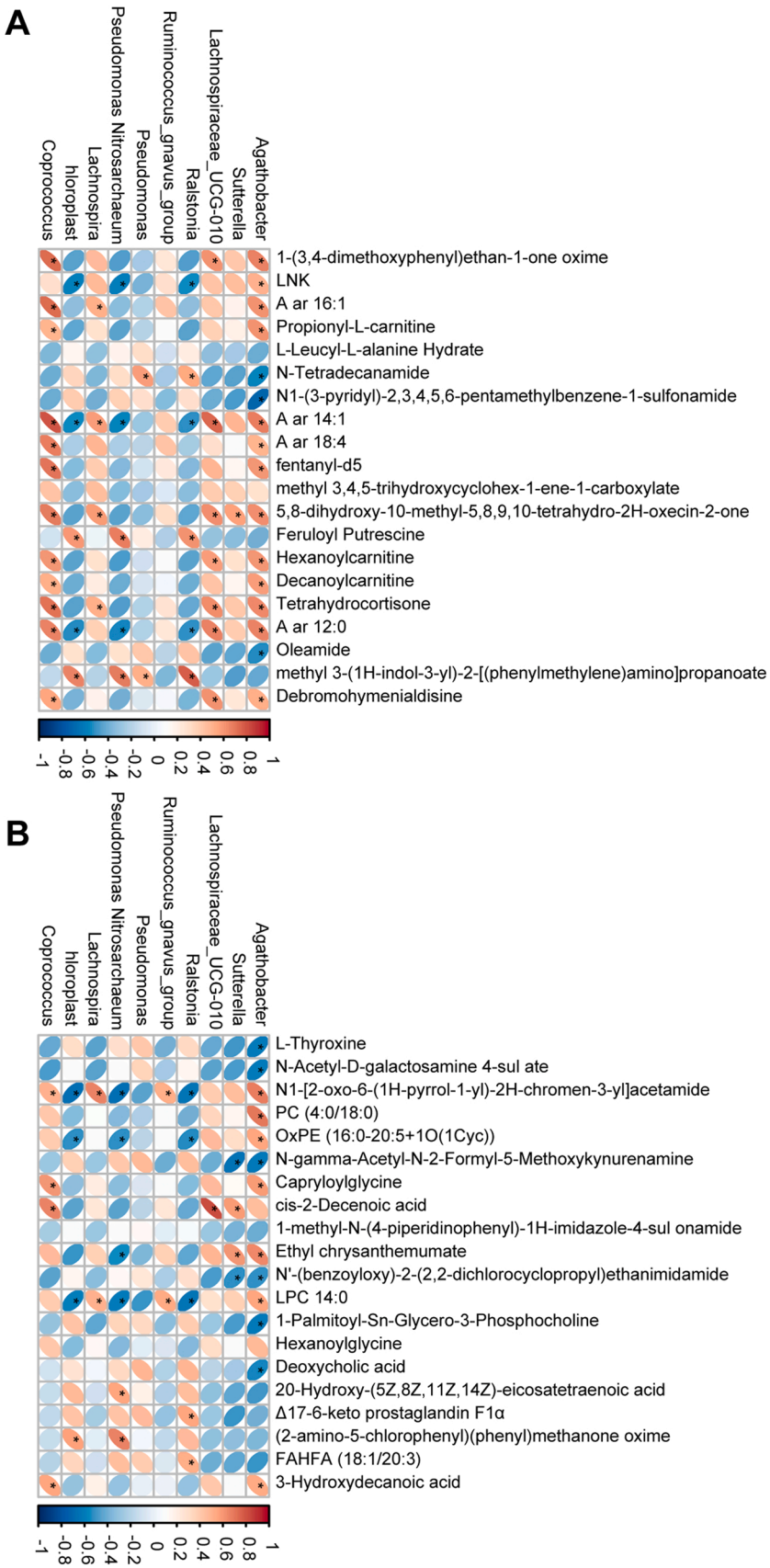

Fig. 6. The correlation analysis between blood metabolome and gut microbiota. (A) The correlation analysis between top 10 gut microbiota and top 20 differential pos metabolites. (B) The correlation analysis between top 10 gut microbiota and top 20 differential neg metabolites; Red means positive correlation, blue means negative correlation; * means p-value < 0.05.

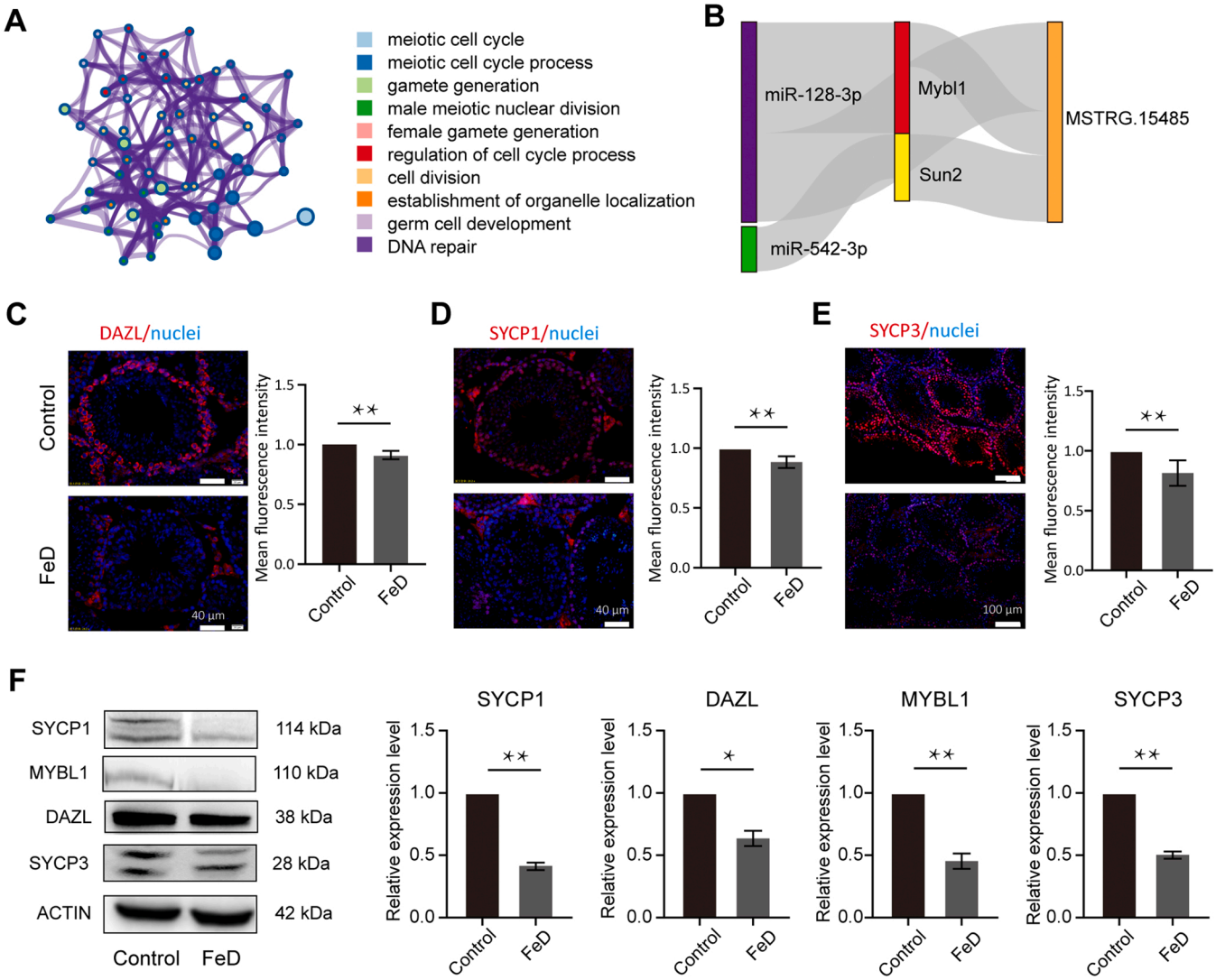

Fig. 7. Insufficient iron intake impairs spermatogenesis by disturbing meiosis. (A) Kyoto Encyclopedia of Genes and Genomes (KEGG) and Gene Ontology (GO) analysis of differentially expressed genes (DEGs) after insufficient iron intake. (B) The Sankey diagram shows the competing endogenous RNA (ceRNA) regulatory mechanism of key genes. (C–E) Immunofluorescence of DAZL, SYCP1 and SYCP3 (red) in the control and iron deficiency (FeD) groups. Hoechst 33342 (blue) was used to stain nuclei. The scale bar is 100 μm. The right panel represents the average fluorescence density of the proteins in each group. (F) Western blotting of the spermatogenesis-related proteins SYCP1, DAZL, MYBL1 and SYCP3. The bar graph shows the relative protein expression level. The results were showed as mean ± SEM (n ≥ 3); * $p < 0.05$, ** $p < 0.01$ *vs.* the control group.

MSTRG.15485 axes exerted a negative effect on spermatogenesis in the presence of iron deficiency (Fig. 7B). The transcriptomic and RT-qPCR data showed consistent data for *miR-128–3p*, *miR-542–3p*, *MSTRG.15485*, *Mybl1* and *Sun2* (Fig. S4B). With iron deficiency, the immunofluorescence analysis showed that DAZL, SYCP1 and SYCP3 levels were decreased (Fig. 7C–E). Western blotting showed a downward expression trend for SYCP1, SYCP3, DAZL and MYBL1 (Fig. 7F).

4. Discussion

Male infertility, characterised by low sperm production, abnormal sperm function or blocked insemination, has gradually emerged as a major issue (Bracke et al., 2018). There are many reasons for male infertility, including congenital factors, such as testicular dysplasia, and acquired factors, such as abnormal metabolism of trace elements (Agarwal et al., 2021). Iron is a key trace element associated with male testicular development, and insufficient or excessive intake can dysregulate spermatogenesis (Wellejus et al., 2000; Madej et al., 2021). However, male reproductive health problems due to iron deficiency are not well understood. Our study highlights the characteristics of spermatogenesis dysfunction induced by iron deficiency, including transcriptomics, metabolomics and microbiomics. Our findings expand previous insights on spermatogenesis dysfunction induced by iron deficiency and provide a novel molecular mechanism represented by ceRNA networks. The common theme that emerges from our current and previous studies is that moderate intake of iron is key to ensure male fertility.

We showed that iron deficiency impaired spermatogenesis, including a decreased sperm concentration, destruction of testicular structure and damage to germ cells (Fig. 1). Mechanistically, defects in these activities appear to be a consequence of transcriptional mis-regulation of genes essential for testicular development. Moreover, iron deficiency impairs spermatogenesis indirectly by affecting hormone synthesis and testicular microbial homeostasis, evidenced by the DEGs, differentially expressed metabolites and functional prediction of differentially expressed microbiota (Zhang et al., 2022; Babakhanzadeh et al., 2020). Although we have deeply analysed the harm exerted by iron deficiency on spermatogenesis from different angles and have identified the

regulation of ceRNA networks, we have not identified the key genes that are affected by iron deficiency and lead to spermatogenesis disorders. Therefore, future research should focus on this direction.

Disturbances in the gut microbiome have been reported to affect spermatogenesis (Ding et al., 2020). Interestingly, we found that iron deficiency produced marked disturbances to the intestinal microbiota, and these disturbances dysregulated spermatogenesis. The extracts and exudates of Cyanobacteria have oestrogenic activity (Sychrová et al., 2012) and reduced sperm motility of the quagga mussel (*Dreissena rostriformis bugensis*) (Boegehold et al., 2019). The evidence suggests that Cyanobacteria is detrimental to spermatogenesis; however, we surprisingly found that the presence of Cyanobacteria is vital for normal spermatogenesis, as it was barely detectable in the gut of iron-deficient mice.

Sertoli cells, Leydig cells and hormones generated by the hypothalamic–pituitary–gonadal axis is critical for regulating sperm production (Corradi et al., 2016). CYP17A1 is a key enzyme in the synthesis of androgen and oestrogen, and its abnormal expression can cause Leydig cell dysfunction (Lardone et al., 2018). We found that *Cyp17a1* deficiency resulted in a significant decline in T production (Yang et al., 2021). Consistent with previous studies, we found that reduced CYP17A1 expression due to iron deficiency is one of the causes of spermatogenesis disturbance. STAR plays an important role in steroidogenesis (Stocco, 2000). Previous research has reported delayed sperm maturation and premature ovarian failure occur in *Star*-null mice (Hasegawa et al., 2000). Consistent with the reported studies, we found that iron deficiency decreased STAR expression, and metabolomic data showed a significant decrease in gonadal hormone levels (Katragadda et al., 2021).

We found that iron deficiency directly impaired meiosis (Fig. 7). Iron deficiency caused a marked downregulation of two key regulators of meiosis, myeloblastosis oncogene-like 1 (*Mybl1*), which is involved in regulating multiple processes in spermatocytes (Bolcun-Filas et al., 2011), and Sad1 and UNC84 domain containing 2 (*Sun2*), which participates in telomere attachment (Alsheimer et al., 2014). Moreover, the disruption of *Sycp1* and *Sycp3*, which are part of the meiotic–synaptic complex, was confirmed by western blotting and immunofluorescence (Syrjänen et al., 2014; Wang et al., 2020). Indeed, by building a ceRNA network, we found some noncoding RNAs, including miRNAs and lncRNAs, that dysregulate spermatogenesis (Li et al., 2020).

Above all, our work highlights the influence of iron deficiency on spermatogenesis. First, iron deficiency directly alters the expression of spermatogenesis-related genes. In addition, abnormal gut microbiota and hormone synthesis caused by iron deficiency can indirectly impair spermatogenesis. We have constructed a three-dimensional network of mechanisms by which iron deficiency affects spermatogenesis by analysing transcriptomic, metabolomic and microbiomic data (Fig. S4C).

5. Conclusion

The present study extends the previous understanding of the iron deficiency and indicates that iron deficiency impairs spermatogenesis by gut-hormone synthesis axis.

Funding

This work was supported by High level talents research fund project of Qingdao Agricultural University in China (1120043) and Taishan Scholar Construction Foundation of Shandong Province (ts20190946).

CRediT authorship contribution statement

Xi-Feng Zhang and Wei Shen designed the study and managed funding; Fa-Li Zhang performed bioinformatic analysis; Shuai Yuan, Pei-Yu Dong and Hao-Hai Ma performed experiments. Massimo De Felici discussed the manuscript. All authors draft and approved the final manuscript.

Declaration of Competing Interest

The authors declare that they have no known competing financial interests or personal relationships that could have appeared to influence the work reported in this paper.

Data availability

Data will be made available on request.

Acknowledgements

We thank all members of Zhang's lab for their contributions to this project.

Consent for publication

All authors approved the final manuscript and agreed to publish.

Appendix A. Supporting information

Supplementary data associated with this article can be found in the online version at doi:10.1016/j.ecoenv.2022.114344.

References

Agarwal, A., Baskaran, S., Parekh, N., Cho, C.-L., Henkel, R., Vij, S., Arafa, M., Selvam, M. K.P., Shah, R., 2021. Male infertility. Lancet 397, 319–333.
Akhter, M.S., Hamali, H.A., Iqbal, J., Mobarki, A.A., Rashid, H., Dobie, G., Madkhali, A. M., Arishi, B.Y., Ageeli, E.O., Laghbi, O.S., 2021. Iron deficiency anemia as a factor in male infertility: awareness in health college students in the Jazan Region of Saudi Arabia. Int. J. Environ. Res. Public Health 18, 12866.
Alsheimer, M., Link, J., Leubner, M., Schmitt, J., Göb, E., Benavente, R., Jeang, K.-T., and Xu, R., 2014, Analysis of Meiosis in SUN1 Deficient Mice Reveals a Distinct Role of SUN2 in Mammalian Meiotic LINC Complex Formation and Function.
Andrews, S., 2010, FastQC: a quality control tool for high throughput sequence data. Babraham Bioinformatics, Babraham Institute, Cambridge, United Kingdom.
Babakhanzadeh, E., Nazari, M., Ghasemifar, S., Khodadadian, A., 2020. Some of the factors involved in male infertility: a prospective review. Int. J. Gen. Med. 13, 29.
Boegehold, A.G., Alame, K., Johnson, N.S., Kashian, D.R., 2019. Cyanobacteria reduce motility of quagga mussel (Dreissena rostriformis bugensis) sperm. Environ. Toxicol. Chem. 38, 368–374.
Bolcun-Filas, E., Bannister, L.A., Barash, A., Schimenti, K.J., Hartford, S.A., Eppig, J.J., Handel, M.A., Shen, L., Schimenti, J.C., 2011. A-MYB (MYBL1) transcription factor is a master regulator of male meiosis. Development 138, 3319–3330.
Bolyen, E., Rideout, J.R., Dillon, M.R., Bokulich, N.A., Abnet, C.C., Al-Ghalith, G.A., Alexander, H., Alm, E.J., Arumugam, M., Asnicar, F., 2019. Reproducible, interactive, scalable and extensible microbiome data science using QIIME 2. Nat. Biotechnol. 37, 852–857.
Bracke, A., Peeters, K., Punjabi, U., Hoogewijs, D., Dewilde, S., 2018. A search for molecular mechanisms underlying male idiopathic infertility. Reprod. Biomed. Online 36, 327–339.
Chen, L., Wang, J., Liu, J., Wang, H., Hillyer, C.D., Blanc, L., An, X., Mohandas, N., 2021. Dynamic changes in murine erythropoiesis from birth to adulthood: implications for the study of murine models of anemia. Blood Adv. 5, 16–25.
Chen, S., Zhou, Y., Chen, Y., Gu, J., 2018. fastp: an ultra-fast all-in-one FASTQ preprocessor. Bioinformatics 34, i884–i890.
Corradi, P.F., Corradi, R.B., Greene, L.W., 2016. Physiology of the hypothalamic pituitary gonadal axis in the male. Urol. Clin. 43, 151–162.
Ding, N., Zhang, X., Di Zhang, X., Jing, J., Liu, S.S., Mu, Y.P., Peng, L.L., Yan, Y.J., Xiao, G.M., Bi, X.Y., 2020. Impairment of spermatogenesis and sperm motility by the high-fat diet-induced dysbiosis of gut microbes. Gut 69, 1608–1619.
Dobin, A., Davis, C.A., Schlesinger, F., Drenkow, J., Zaleski, C., Jha, S., Batut, P., Chaisson, M., Gingeras, T.R., 2013. STAR: ultrafast universal RNA-seq aligner. Bioinformatics 29, 15–21.
Douglas, G.M., Maffei, V.J., Zaneveld, J.R., Yurgel, S.N., Brown, J.R., Taylor, C.M., Huttenhower, C., Langille, M.G., 2020. PICRUSt2 for prediction of metagenome functions. Nat. Biotechnol. 38, 685–688.
Guo, H., Ouyang, Y., Yin, H., Cui, H., Deng, H., Liu, H., Jian, Z., Fang, J., Zuo, Z., Wang, X., 2022. Induction of autophagy via the ROS-dependent AMPK-mTOR pathway protects copper-induced spermatogenesis disorder. Redox Biol. 49, 102227.
Hasegawa, T., Zhao, L., Caron, K.M., Majdic, G., Suzuki, T., Shizawa, S., Sasano, H., Parker, K.L., 2000. Developmental roles of the steroidogenic acute regulatory protein (StAR) as revealed by StAR knockout mice. Mol. Endocrinol. 14, 1462–1471.

Kang, Y.-J., Yang, D.-C., Kong, L., Hou, M., Meng, Y.-Q., Wei, L., Gao, G., 2017. CPC2: a fast and accurate coding potential calculator based on sequence intrinsic features. Nucleic Acids Res. 45, W12–W16.
Katragadda, V., Adem, M., Mohammad, R.A., Sri Bhasyam, S., Battini, K., 2021. Testosterone recuperates deteriorated male fertility in cypermethrin intoxicated rats. Toxicol. Res. 37, 125–134.
Khanehzad, M., Abbaszadeh, R., Holakuyee, M., Modarressi, M.H., Nourashrafeddin, S. M., 2021. FSH regulates RA signaling to commit spermatogonia into differentiation pathway and meiosis. Reprod. Biol. Endocrinol. 19, 1–19.
Killip, S., Bennett, J.M., Chambers, M.D., 2007. Iron deficiency anemia. Am. Fam. Physician 75, 671–678.
Kong, L., Zhao, A.-H., Wang, Q.-W., Feng, Y.-Q., Yan, Z.-H., Li, M.-H., Zhang, F.-L., Wang, H., Shen, K.-Y., Liu, Y., 2021. Maternal Zearalenone exposure impacted ovarian follicle formation and development of suckled offspring. Sci. Total Environ. 788, 147792.
Lardone, M., Argandoña, F., Lorca, M., Piottante, A., Flórez, M., Palma, C., Ebensperger, M., Castro, A., 2018. Leydig cell dysfunction is associated with post-transcriptional deregulation of CYP17A1 in men with Sertoli cell-only syndrome. MHR: Basic Sci. Reprod. Med. 24, 203–210.
Li, N., Liu, X.-L., Zhang, F.-L., Tian, Y., Zhu, M., Meng, L.-Y., Dyce, P.W., Shen, W., Li, L., 2020. Whole-transcriptome analysis of the toxic effects of zearalenone exposure on ceRNA networks in porcine granulosa cells. Environ. Pollut. 261, 114007.
Liao, Y., Smyth, G.K., Shi, W., 2014. featureCounts: an efficient general purpose program for assigning sequence reads to genomic features. Bioinformatics 30, 923–930.
Ling, Y., Xu, L., Zhu, L., Sui, M., Zheng, Q., Li, W., Liu, Y., Fang, F., Zhang, X., 2017. Identification and analysis of differentially expressed long non-coding RNAs between multiparous and uniparous goat (Capra hircus) ovaries. PloS One 12, e0183163.
Love, M.I., Huber, W., Anders, S., 2014. Moderated estimation of fold change and dispersion for RNA-seq data with DESeq2. Genome Biol. 15, 1–21.
Madej, D., Pietruszka, B., Kaluza, J., 2021. The effect of iron and/or zinc diet supplementation and termination of this practice on the antioxidant status of the reproductive tissues and sperm viability in rats. J. Trace Elem. Med. Biol. 64, 126689.
Nishimura, H., L'Hernault, S.W., 2017. Spermatogenesis. Curr. Biol. 27, R988–R994.
Peng, Z., Yang, Q., Yeerken, R., Chen, J., Liu, X., Li, X., 2022. Multi-omics analyses reveal the mechanisms of Arsenic-induced male reproductive toxicity in mice. J. Hazard. Mater. 424, 127548.
Pertea, M., Pertea, G.M., Antonescu, C.M., Chang, T.-C., Mendell, J.T., Salzberg, S.L., 2015. StringTie enables improved reconstruction of a transcriptome from RNA-seq reads. Nat. Biotechnol. 33, 290–295.
Song, S., Yang, L., Ye, M., Chen, X., Shi, F., Shaikh, F., 2016. Antioxidant activity of a Lachnum YM226 melanin–iron complex and its influence on cytokine production in mice with iron deficiency anemia. Food Funct. 7, 1508–1514.
Stocco, D., 2000. The role of the StAR protein in steroidogenesis: challenges for the future. J. Endocrinol. 164, 247–253.
Sun, L., Luo, H., Bu, D., Zhao, G., Yu, K., Zhang, C., Liu, Y., Chen, R., Zhao, Y., 2013. Utilizing sequence intrinsic composition to classify protein-coding and long non-coding transcripts. Nucleic Acids Res. 41 e166-e166.
Sychrová, E., Štěpánková, T., Nováková, K., Bláha, L., Giesy, J.P., Hilscherová, K., 2012. Estrogenic activity in extracts and exudates of cyanobacteria and green algae. Environ. Int. 39, 134–140.
Syrjänen, J.L., Pellegrini, L., Davies, O.R., 2014. A molecular model for the role of SYCP3 in meiotic chromosome organisation. Elife 3, e02963.
Wang, J.-J., Ge, W., Zhai, Q.-Y., Liu, J.-C., Sun, X.-W., Liu, W.-X., Li, L., Lei, C.-Z., Dyce, P.W., De Felici, M., 2020. Single-cell transcriptome landscape of ovarian cells during primordial follicle assembly in mice. PLoS Biol. 18, e3001025.
Wellejus, A., Poulsen, H.E., Loft, S., 2000. Iron-induced oxidative DNA damage in rat sperm cells in vivo and in vitro. Free Radic. Res. 32, 75–83.
Wu, T., Hu, E., Xu, S., Chen, M., Guo, P., Dai, Z., Feng, T., Zhou, L., Tang, W., Zhan, L., 2021. clusterProfiler 4.0: A universal enrichment tool for interpreting omics data. Innovation 2, 100141.
Yang, L., Zhang, X., Liu, S., Zhao, C., Miao, Y., Jin, L., Wang, D., Zhou, L., 2021. Cyp17a1 is required for female sex determination and male fertility by regulating sex steroid biosynthesis in fish. Endocrinology 162, bqab205.
Zhang, F.-L., Li, N., Wang, H., Ma, J.-M., Shen, W., Li, L., 2019. Zearalenone exposure induces the apoptosis of porcine granulosa cells and changes long noncoding RNA expression to promote antiapoptosis by activating the JAK2–STAT3 pathway. J. Agric. Food Chem. 67, 12117–12128.
Zhang, P., Feng, Y., Li, L., Ge, W., Yu, S., Hao, Y., Shen, W., Han, X., Ma, D., Yin, S., 2021. Improvement in sperm quality and spermatogenesis following faecal microbiota transplantation from alginate oligosaccharide dosed mice. Gut 70, 222–225.
Zhang, T., Sun, P., Geng, Q., Fan, H., Gong, Y., Hu, Y., Shan, L., Sun, Y., Shen, W., Zhou, Y., 2022. Disrupted spermatogenesis in a metabolic syndrome model: the role of vitamin A metabolism in the gut–testis axis. Gut 71, 78–87.
Zhou, Y., Zhou, B., Pache, L., Chang, M., Khodabakhshi, A.H., Tanaseichuk, O., Benner, C., Chanda, S.K., 2019. Metascape provides a biologist-oriented resource for the analysis of systems-level datasets. Nat. Commun. 10, 1–10.